

Modeling, Analysis, and Hard Real-time Scheduling of Adaptive Streaming Applications

Jiali Teddy Zhai, Sobhan Niknam, and Todor Stefanov, *Member, IEEE*

Abstract—In real-time systems, the application’s behavior has to be predictable at compile-time to guarantee timing constraints. However, modern streaming applications which exhibit adaptive behavior due to mode switching at run-time, may degrade system predictability due to unknown behavior of the application during mode transitions. Therefore, proper temporal analysis during mode transitions is imperative to preserve system predictability. To this end, in this paper, we initially introduce Mode Aware Data Flow (MADF) which is our new predictable Model of Computation (MoC) to efficiently capture the behavior of adaptive streaming applications. Then, as an important part of the operational semantics of MADF, we propose the Maximum-Overlap Offset (MOO) which is our novel protocol for mode transitions. The main advantage of this transition protocol is that, in contrast to self-timed transition protocols, it avoids timing interference between modes upon mode transitions. As a result, any mode transition can be analyzed independently from the mode transitions that occurred in the past. Based on this transition protocol, we propose a hard real-time analysis as well to guarantee timing constraints by avoiding processor overloading during mode transitions. Therefore, using this protocol, we can derive a lower bound and an upper bound on the earliest starting time of the tasks in the new mode during mode transitions in such a way that hard real-time constraints are respected.

I. INTRODUCTION

TO handle the ever-increasing computational demands and meet hard real-time constraints in streaming applications, where the huge amount of streaming data should be processed in a short time interval, embedded systems have relied on Multi-Processor System-on-Chip (MPSoC) platforms to benefit from parallel processing. To efficiently exploit the computational capacity of MPSoCs, however, streaming applications must be expressed primarily in a parallel fashion. The common practice for expressing the parallelism in an application is to use parallel Models of Computation (MoCs) [1]. Within a parallel MoC, a streaming application is modeled as a directed graph, where graph nodes represent actors (i.e., tasks) and graph edges represent data dependencies. Actors are executed concurrently and communicate data explicitly via FIFOs. For example, Synchronous Data Flow (SDF) [2] and Cyclo-Static Data Flow (CSDF) [3] are two popular parallel MoCs because of their compile-time analyzability. Due to the static nature of SDF and CSDF MoCs, the actors are restricted to produce and

consume data with fixed rates per firing or, in case of CSDF, with fixed periodic patterns.

Nowadays, many modern streaming applications, in the domain of multimedia, image, and signal processing, increasingly show adaptive behavior at run-time. For example, a computer vision system processes different parts of an image continuously to obtain information from several regions of interest depending on the actions taken by the external environment. This adaptive behavior, however, cannot be effectively expressed with an SDF or CSDF model due to their limited expressiveness. As a result, more expressive models, e.g., Scenario-Aware Data Flow (SADF) [4], Finite State Machine (FSM)-based Scenario-Aware Data Flow (FSM-SADF) [5], Variable-rate Phased Data Flow (VPDF) [6], and Mode-controlled Data Flow (MCDF) [7], have been proposed and deployed as extensions of the (C)SDF model. These MoCs are able to capture the behavior of an adaptive streaming application as a collection of different static behaviors, called scenarios or modes, which are individually predictable in performance and resource usage at compile-time.

Moreover, to guarantee tight timing constraints in modern streaming applications with adaptive behavior nature, proper temporal analysis for application execution during mode transitions, when the application’s behavior is switching from one mode to another mode, is imperative at compile-time. However, such analysis can be difficult due to the fact that different actors in different modes are concurrently executing during mode transitions. This difficulty comes directly from the protocol adopted for the mode transitions. In the existing adaptive MoCs, like MCDF [7] and FSM-SADF [5], a protocol, referred as self-timed transition protocol, has been adopted which specifies that actors are scheduled as soon as possible not only in each mode individually, but also during mode transitions. This protocol, however, introduces interference of one mode execution with another one, as explained in Section IV-C1. As a consequence, the temporal analysis of a mode transition is tightly dependent on the mode transitions that occurred in the past. Another consequence of the incurred interference between modes is the high time complexity of analyzing mode transitions, as the mode transitions cannot be analyzed independently, e.g., see the state-space exploration approach proposed in [5].

Therefore, to overcome the aforementioned interference issue and consequent problems caused by the self-timed transition protocol, in this paper, we propose a new MoC called Mode Aware Data Flow (MADF) to model adaptive streaming applications, that is armed by a novel transition protocol called Maximum-Overlap Offset. This transition protocol enables an independent analysis for mode transitions. The specific novel contributions of this paper are the following:

This article was presented in the International Conference on Embedded Software 2018 and appears as part of the ESWEEK-TCAD special issue.

The authors contributed to the paper equally. The authors are with the Leiden Institute of Advanced Computer Science, Leiden University, Leiden, The Netherlands, Email: teddyzhai@gmail.com, {s.niknam,t.p.stefanov}@liacs.leidenuniv.nl. This research is supported by the Dutch Technology Foundation STW under the Robust Cyber Physical Systems program (Project 12695).

- We propose a new MoC, Mode-Aware Data Flow (MADF), that has the advantages of SADF [4] and VPDF [6]. Inspired by SADF, we characterize the behavior of adaptive streaming applications with individual modes and transitions between them. Similar to VPDF, the length of production/consumption sequences for an actor varies from one mode to another. The length is only fixed when the mode is known. Then, based on the clear distinction between modes and transitions, we define analyzable operational semantics for MADF;
- As an important part of the operational semantics of MADF, we propose the Maximum-Overlap Offset (MOO) which is our novel protocol for mode transitions. The main advantage of this transition protocol is that, in contrast to the self-timed transition protocol, adopted in [5], [7], it avoids timing interference between modes upon mode transitions. As a result, this transition protocol enables an independent analysis for mode transitions. This means, the analysis of any mode transition is independent from the mode transitions that occurred in the past. This independent analysis significantly reduces the complexity of the analysis as the complexity merely depends on the number of allowed transitions. This is crucial for applications with a large number of modes and possible transitions;
- Based on the novel MOO transition protocol, we propose a hard real-time analysis approach to guarantee the timing constraints by avoiding processor overloading, i.e., avoiding that the total utilization of allocated tasks on a processor exceeds its capacity, during mode transitions. Our analysis is much simpler and faster than the computationally intensive state-of-the-art timing analysis approaches such as [5].

The remainder of this paper is organized as follows: Section II gives an overview of the related work. Section III introduces the background needed for understanding the contributions of this paper. Our novel adaptive MoC and transition protocol are then introduced in Section IV. Based on the novel transition protocol, in Section V, we present our hard real-time analysis approach to guarantee the timing constraints during mode transitions. In Section VI, two case studies are presented to illustrate the practical applicability of our proposed MADF mode, transition protocol, and real-time analysis. Finally, Section VII ends the paper with conclusions.

II. RELATED WORK

To model the adaptive behavior of modern streaming applications while having certain degree of compile-time analyzability, different MoCs such as Scenario-Aware Data Flow (SADF) [4], Finite State Machine (FSM)-based Scenario-Aware Data Flow (FSM-SADF) [5], Variable-rate Phased Data Flow (VPDF) [6], Mode-controlled Data Flow (MCDF) [7], and Parameterized SDF (PSDF) [8] have been already proposed in the literature.

In SADF [4] and FSM-SADF [5], *detector* actors are introduced to parameterize the SDF model. All valid scenarios and their possible order of occurrence, which is shown either by using a Markov chain [4] or finite state machine [5], must

be predefined at compile-time. Each scenario consists of a set of valid parameter combination that determines a scenario of SADF. This guarantees the consistency of SADF in individual scenarios, therefore, no run-time consistency check is required. In a scenario, the SADF model behaves the same way as the SDF model. Therefore, an SADF graph can be seen as a set of SDF graphs. In the initial FSM-SADF definition, all the production and consumption rates of the data-flow edges are constant within a graph iteration of a scenario.

For the FSM-SADF MoC [5], the authors proposed an approach to compute worst-case performance among all mode transitions, assuming the self-timed transition protocol. Although it is an exact analysis, the approach has inherently exponential time complexity. Moreover, this approach leads to timing interference between modes upon mode transitions. In contrast, our approach does not introduce interference between modes due to the novel MOO transition protocol proposed in Section IV-C2. The timing behavior of individual modes and during mode transitions can be analyzed independently. In addition, our approach considers allocation of actors on processors, which by itself is a harder problem than the one addressed in [5].

In [9], the author proposes to use a linear model to capture worst-case transition delay and period during scenario transitions of FSM-SADF. Our transition protocol is conceptually similar to the linear model. However, we obtain the linear model in a different way, specifically simplified for the adopted hard real-time scheduling framework. For instance, finding a reference schedule is not necessary in our case, but being crucial in the tightness of the analysis proposed in [9]. Moreover, our approach solves the problem of changing the application graph structure during mode transitions, which was not studied in [9].

For VPDF [6], the analysis has been limited to computing buffer sizes under throughput constraints so far. The execution of a VPDF graph on MPSoC platforms under hard real-time constraints has not been studied. In particular, the allocation of actors and how to switch from one mode to another one are not discussed. Moreover, delay due to mode transitions has not been investigated. Our approach, on the other hand, takes these important factors into account. Therefore, our analysis results are directly reflected in a real implementation.

MCDF [7] is another adaptive MoC which properties can be partly analyzed at compile-time. The MCDF MoC primarily focuses on Software-Defined Radio applications, where different sub-graphs need to be active in different modes. This is achieved by using *switch* and *select* actors. The author implicitly assumes self-timed scheduling during mode transitions. Based on this assumption, a worst-case timing analysis is developed. Similar to the case of SADF, the use of the self-timed scheduling introduces timing interference between modes. As a consequence, the analysis must take into account the sequence of mode transitions of interest. Although the author provides an upper bound of timing behavior for a parameterized sequence of mode transitions, the accuracy is still unknown. In contrast, our approach results in a timing analysis of mode transitions that is independent from already occurred transitions. Moreover, the analysis results are directly

reflected in the final implementation. In this sense, our analysis is exact in the timing behavior of mode transitions.

In [8], a meta-modeling technique is proposed to augment the expressive power of wide range of existing data-flow models which have the graph iteration concept. In [8], the proposed technique is especially applied to the SDF model which is called Parameterized SDF (PSDF). In PSDF, separate *init* and *sub-init* graphs are proposed to reconfigure the body graph in a hierarchical manner. In this model, functional properties can only be partially decided at compile-time, and thus run-time verification is needed. To this end, for all configurations, computing a schedule and verifying consistency for both graphs and specifications need to be fulfilled at run-time which is pretty complex procedure. In addition, temporal analysis to find the worst-case system reconfiguration delay to preserve model predictability is not proposed. In contrast, our MADF model does not require run-time consistency check as every mode in our model is predefined at compile-time and represented as a CSDF graph. In addition, our MADF provides the temporal analysis of the mode transitions at compile-time using the MOO transition protocol.

In [10], [11], an analysis is proposed to reason about worst-case response time of a task graph in case of a mode change. However, the task graph has very limited expressiveness and is not able to model the behavior of adaptive streaming applications. Instead, in our paper, we define a more expressive MoC that is amenable to adaptive application behavior and real-time analysis.

In [12], [13], the authors focus on timing analysis for mode changes of real-time tasks. The starting times of new mode tasks need to be delayed to avoid overloading of processors during mode changes. In [12], [13], however, it is assumed that tasks are independent. The proposed algorithms are thus not applicable to adaptive MoCs, since the starting times of tasks in adaptive MoCs depend on each other due to data dependencies. Moreover, the algorithms in [12], [13] involve high computational complexity because fixed-point equations must be solved at every step in the algorithms. In contrast, in our paper, we propose an adaptive MoC and analysis for applications with data-dependent tasks, which is more realistic and applicable to wider range of real-life streaming applications. Moreover, our analysis is simpler with low computational and time complexity.

III. BACKGROUND

In this section, we provide a brief overview of our system model, the CSDF MoC, and the scheduling framework presented in [14]. This background is needed to understand the novel contributions of our work.

A. System Model

The considered MPSoC platforms in this work are homogeneous, i.e., they may contain multiple, but the same type of programmable Processing Elements (PEs) with distributed memories. Moreover, the platform must be predictable, which means timing guarantees are provided on the response time of hardware components and OS schedulers. The precision-timed

(PRET) [15] platform is such an example. On the software side, we assume partitioned scheduling algorithms, i.e, no migration of tasks between PEs is allowed. The considered scheduling algorithms on each PE include Fixed-Priority Preemptive Scheduling (FPPS) algorithms, such as RM [16], or dynamic scheduling algorithms, such as EDF [16].

B. Cyclo-Static Data Flow (CSDF)

An application modeled as a CSDF [3] is defined as a directed graph $G = (\mathcal{A}, \mathcal{E})$ that consists of a set of actors \mathcal{A} which communicate with each other through a set of edges \mathcal{E} . Actors represent computation while edges represent data dependency due to communication and synchronization. In CSDF, every actor $A_i \in \mathcal{A}$ has an execution sequence $C_i = [c_1, c_2, \dots, c_{\phi_i}]$ of length ϕ_i . This means, the x -th time that actor A_i is fired, it performs the computation $C_i(((x-1) \bmod \phi_i) + 1)$. Similarly, production and consumption of data tokens are also sequences of length ϕ_i in CSDF. The token production of actor A_i to edge E_j is represented as a sequence of constant integers $PRD_j = [prd_1, prd_2, \dots, prd_{\phi_i}]$, called *production sequence*. Analogously, token consumption from every input edge E_k of actor A_i is a predefined sequence $CNS_k = [cns_1, cns_2, \dots, cns_{\phi_i}]$, called *consumption sequence*. The x -th time that actor A_i is fired, it produces $PRD_j(((x-1) \bmod \phi_i) + 1)$ tokens to channel E_j and consumes $CNS_k(((x-1) \bmod \phi_i) + 1)$ tokens from channel E_k .

An important property of the CSDF model is the ability to derive a schedule for the actors at compile-time. In order to derive a valid static schedule for a CSDF graph at compile-time, it has to be consistent and live.

Theorem 1 (From [3]). *In a CSDF graph G , a repetition vector $\vec{q} = [q_1, q_2, \dots, q_{|\mathcal{A}|}]^T$ is given by*

$$\vec{q} = \Theta \cdot \vec{r} \quad \text{with} \quad \Theta_{ji} = \begin{cases} \phi_i & \text{if } j = i \\ 0 & \text{otherwise} \end{cases} \quad (1)$$

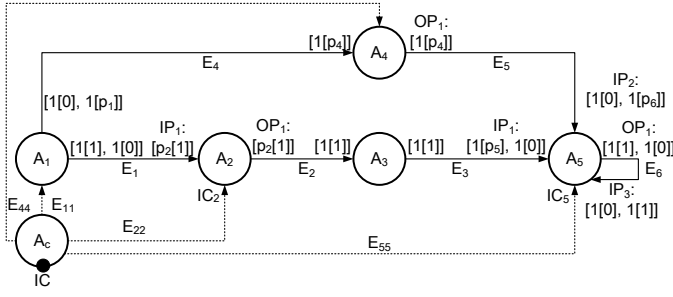
where $\vec{r} = [r_1, r_2, \dots, r_{|\mathcal{A}|}]^T$ is a positive integer solution of the balance equation $\Gamma \cdot \vec{r} = \vec{0}$ and where the topology matrix $\Gamma \in \mathbb{Z}^{|\mathcal{E}| \times |\mathcal{A}|}$ is defined by

$$\Gamma_{ji} = \begin{cases} \sum_{k=1}^{k=\phi_i} PRD_j(k) & \text{if actor } A_i \text{ produces to edge } E_j \\ -\sum_{k=1}^{k=\phi_i} CNS_j(k) & \text{if actor } A_i \text{ consumes from edge } E_j \\ 0 & \text{otherwise.} \end{cases}$$

A CSDF graph G is said to be consistent if a positive integer solution $\vec{r} = [r_1, r_2, \dots, r_{|\mathcal{A}|}]^T$ exists for the balance equation in Equation (1). If a deadlock-free schedule can be found, G is said to be live. Each consistent CSDF graph has a non-trivial repetition vector $\vec{q} = [q_1, q_2, \dots, q_{|\mathcal{A}|}]^T \in \mathbb{N}^{|\mathcal{A}|}$. An entry $q_i \in \vec{q}$ denotes how many times an actor $A_i \in \mathcal{A}$ has to be executed in every graph iteration of G . For more details, we refer the reader to [3].

C. Strictly Periodic Scheduling of CSDF

In [14], a real-time strictly periodic scheduling (SPS) framework for CSDF graphs is proposed. In this framework, the actors in a CSDF graph are converted to a set of real-time implicit-deadline periodic tasks. Therefore, such a real-time task corresponding to a CSDF actor is associated with two

Fig. 1. An example of MADF graph (G_1).

parameters, namely period T and earliest starting time S , where the deadline of the task is equal to its period (i.e., implicit deadline). The minimum period T_i [14] of any actor $A_i \in \mathcal{A}$ under SPS can be computed as:

$$T_i = \frac{lcm(\vec{q}) \lceil \max_{A_i \in \mathcal{A}} \{\mu_i q_i\} \rceil}{q_i} \quad (2)$$

where q_i is the number of repetitions of actor A_i per graph iteration, and μ_i is the worst-case execution time (WCET) of actor A_i . In general, the derived period vector \vec{T} must satisfy the condition $q_1 T_1 = q_2 T_2 = \dots = q_n T_n = H$, where H is the iteration period, also called hyper period, that represents the duration needed by the graph to complete one iteration. The minimum period of the sink actor for a CSDF graph determines the maximum throughput that this graph can achieve. In addition, the utilization of any actor $A_i \in \mathcal{A}$, denoted by u_i , can be computed as $u_i = \mu_i / T_i$, where $u_i \in (0, 1]$.

To sustain a strictly periodic execution with the period derived by Equation (2), the earliest starting time S_i [14] of any actor $A_i \in \mathcal{A}$ can be obtained as:

$$S_i = \begin{cases} 0 & \text{if } \text{prec}(A_i) = \emptyset \\ \max_{A_j \in \text{prec}(A_i)} (S_{j \rightarrow i}) & \text{otherwise,} \end{cases} \quad (3)$$

where $\text{prec}(A_i)$ represents the set of predecessor actors of A_i and $S_{j \rightarrow i}$ is given by:

$$S_{j \rightarrow i} = \min_{t \in [0, S_j + H]} \left\{ t : \begin{array}{l} \text{Prd}_{[t, t_e]}(A_j, E_u) \\ \geq \text{Cns}_{[t, t_e]}(A_i, E_u), \forall k \in [0, H], k \in \mathbb{N} \end{array} \right\} \quad (4)$$

where $\text{Prd}_{[t_s, t_e]}(A_j, E_u)$ is the total number of tokens produced by A_j to edge E_u during the time interval $[t_s, t_e]$ and $\text{Cns}_{[t_s, t_e]}(A_i, E_u)$ is the total number of tokens consumed by A_i from edge E_u during the time interval $[t_s, t_e]$. Equation (4) considers the dependency between actors A_j and A_i , over directed channel E_u . It calculates the earliest starting time $S_{j \rightarrow i}$ such that A_i is never blocked on reading data tokens from E_u during its periodic execution. This is ensured by checking that at each time instant, actor A_i can be fired such that the cumulative number of tokens produced by A_j over E_u is greater than or equal to the number of tokens A_i consumes from E_u . Start times $S_{j \rightarrow i}$ are computed for each actor A_j in the predecessor set of A_i , i.e., $A_j \in \text{prec}(A_i)$. Then, when actor A_i has several predecessors, the earliest starting time S_i has to be set to the maximum of starting times $S_{j \rightarrow i}$ considering each predecessor in isolation, as captured by Equation (3). For more details, we refer the reader to [14].

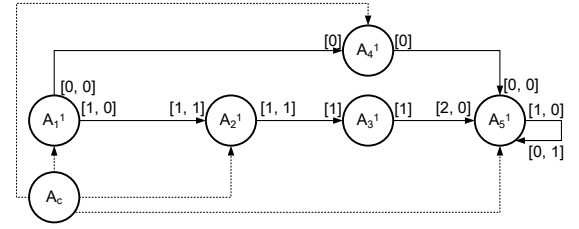
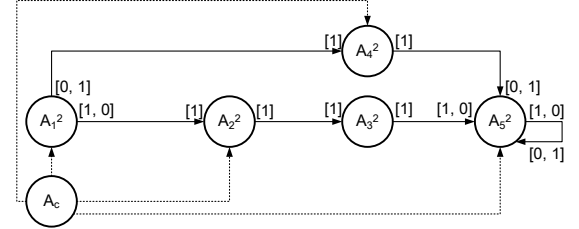
(a) CSDF graph G_1^1 of mode S^1 .(b) CSDF graph G_1^2 of mode S^2 .

Fig. 2. Two modes of the MADF graph in Fig. 1.

IV. MODE-AWARE DATA FLOW (MADF)

In this section, we introduce our new MoC called Mode-Aware Data Flow (MADF). MADF can capture multiple modes associated with an adaptive streaming application, where each individual mode is a CSDF graph [3]. Details and formal definitions of the MADF model and its operational semantics are given later in this section. Here, we explain the MADF intuitively by an example. Throughout this paper, we use graph G_1 shown in Fig. 1 as the running example to illustrate the definition of MADF and the hard real-time scheduling analysis related to MADF. This graph consists of 5 computation actors A_1 to A_5 that communicate data over edges E_1 to E_5 . Also, there is an extra actor A_c which controls the switching between modes through control edges E_{11} , E_{22} , E_{44} , and E_{55} at run-time. Each edge contains a production and a consumption pattern, and some of these production and consumption patterns are parameterized. Having different values of parameters and worst-case execution times (WCET) of the actors determine different modes. For example, to specify the consumption pattern with variable length on edge E_1 in graph G_1 , the parameterized notation $[p_2[1]]$ is used on edge E_1 that is interpreted as a sequence of p_2 elements with integer value 1, e.g., $[2[1]] = [1, 1]$. Similarly, the notation $[1[p_4]]$ on edge E_4 is interpreted as a sequence of 1 element with integer value p_4 , e.g., $[1[2]] = [2]$. Assume in this particular example that parameter vector $(p_1, p_2, p_4, p_5, p_6)$ can take only two values $(0, 2, 0, 2, 0)$ and $(1, 1, 1, 1, 1)$. Then, A_c can switch the application between two corresponding modes S^1 and S^2 by setting the parameter vector to value $(0, 2, 0, 2, 0)$ and $(1, 1, 1, 1, 1)$, respectively, at run-time. Fig. 2(a) and (b) show the corresponding CSDF graphs of mode S^1 and S^2 .

A. Formal Definition of MADF

Definition 1 (Mode-Aware Data Flow (MADF)).

A Mode-Aware Data Flow (MADF) is a multi-graph defined by a tuple $(\mathcal{A}, A_c, \mathcal{E}, \Pi)$, where

TABLE I
MAPPING RELATION M_2 FOR ACTOR A_2
IN FIG. 1.

$\vec{p}_2 = [p_2]$	ϕ	\vec{C}_2
2	2	$[c_1, c_2]$
1	1	$[c_3]$

TABLE II
FUNCTION MC_5 DEFINED FOR ACTOR
 A_5 IN FIG. 1.

S	\mathbb{N}^2
SI^1	$[2, 0]$
SI^2	$[1, 1]$

- $\mathcal{A} = \{A_1, \dots, A_{|\mathcal{A}|}\}$ is a set of dataflow actors;
- A_c is the control actor to determine modes and their transitions;
- \mathcal{E} is the set of edges for data/parameter transfer;
- $\Pi = \{\vec{p}_1, \dots, \vec{p}_{|\mathcal{A}|}\}$ is the set of parameter vectors, where each $\vec{p}_i \in \Pi$ is associated with a dataflow actor A_i .

For G_1 , $\mathcal{A} = \{A_1, A_2, A_3, A_4, A_5\}$ is the set of dataflow actors. A_c is the control actor. $\mathcal{E} = \{E_1, E_2, E_3, E_4, E_5, E_6, E_{11}, E_{22}, E_{44}, E_{55}\}$ is the set of edges. For actor A_5 , $\vec{p}_5 = [p_5, p_6]$ is the parameter vector. The input port IP_1 of actor A_5 has a consumption sequence $[1[p_5], 1[0]]$, which can be interpreted as $[p_5, 0]$.

Definition 2 (Dataflow Actor). A dataflow actor A_i is described by a tuple $(\mathcal{I}_i, IC_i, O_i, C_i, M_i)$, where

- $\mathcal{I}_i = \{IP_1, \dots, IP_{|\mathcal{I}_i|}\}$ is the set of data input ports of actor A_i ;
- IC_i is the control input port that reads parameter vector \vec{p}_i for actor A_i ;
- $O_i = \{OP_1, \dots, OP_{|O_i|}\}$ is the set of data output ports of actor A_i ;
- $C_i = \{c_1, \dots, c_{|C_i|}\}$ is the set of computations. When actor A_i fires, it performs a computation $c_k \in C_i$;
- $M_i : \vec{p}_i \rightarrow \{\phi, \vec{C}_i\}$ is a mapping relation, where $\vec{p}_i \in \Pi$, $\phi \in \mathbb{N}^+$, and $\vec{C}_i \subseteq C_i$ is a sequence of computations $[\vec{C}_i(1), \dots, \vec{C}_i(k), \dots, \vec{C}_i(\phi)]$ with $\vec{C}_i(k) \in C_i$, $1 \leq k \leq \phi$.

Actor A_2 in Fig. 1 has a set of one input port $\mathcal{I}_2 = \{IP_1\}$, a set of one output port $O_2 = \{OP_1\}$ as well as a control input port IC_2 . A set of computations $C_2 = \{c_1, c_2, c_3\}$ is associated with A_2 . The mapping relation M_2 is given in Table I. It can be interpreted as follows: If $p_2 = 2$, actor A_2 repetitively performs computations according to sequence $\vec{C}_2 = [c_1, c_2]$ every time when firing A_2 . When $p_2 = 1$, firing A_2 performs computation c_3 .

Definition 3 (Control Actor). The control actor A_c is described by a tuple (IC, O_c, S, M_c) , where

- $S = \{SI^1, \dots, SI^{|\mathcal{S}|}\}$ is a set of mode identifiers, each of which specifies a unique mode;
- IC is the control input port which is connected to the external environment. Mode identifiers are read through the control input port from the environment;
- $O_c = \{OC_1, \dots, OC_{|\mathcal{A}|}\}$ is a set of control output ports. Parameter vector \vec{p}_i is sent through $OC_i \in O_c$ to actor A_i ;
- $M_c = \{MC_1, \dots, MC_{|\mathcal{A}|}\}$ is a set of functions defined for each actor $A_i \in \mathcal{A}$. For each $MC_i \in M_c$, $MC_i : S \rightarrow \mathbb{N}^{|\vec{p}_i|}$ is a function that takes a mode identifier and outputs a vector of non-negative integer values.

For G_1 in Fig. 1, we have two mode identifiers $S = \{SI^1, SI^2\}$. At run-time, control actor A_c reads these mode identifiers

through control port IC (black dot in Fig. 1). For actor A_5 , $MC_5 \in M_c$ is given in Table II. As explained previously, the parameter vector for actor A_5 is $\vec{p}_5 = [p_5, p_6]$. Therefore, MC_5 takes a mode identifier and outputs a 2-dimensional vector as shown in the second column in Table II. For instance, mode SI^1 results in a non-negative integer vector $[2, 0]$.

To further define production/consumption sequences with variable length, we use the notation $n[m]$ for a sequence of n elements with integer value m , i.e.,

$$n[m] = \overbrace{[m, \dots, m]}^{n \text{ times}}.$$

Definition 4 (Input Port). An input port IP of an actor is described by a tuple (CNS, M_{IP}) , where

- $CNS = [\phi_1[cns_1], \dots, \phi_K[cns_K]]$ is the consumption sequence with ϕ phases, where $\phi = \sum_{i=1}^K \phi_i$ is determined by the mapping relation M in Definition 2, and $cns_1, \dots, cns_K \in \mathbb{N}$;
- $M_{IP} : \vec{p}_i \rightarrow \psi_{IP}$ is a mapping relation, where $\vec{p}_i \in \Pi$ and

$$\psi_{IP} = \{\phi_1, \dots, \phi_K, cns_1, \dots, cns_K\}. \quad (5)$$

Definition 5 (Output Port). An output port OP of an actor is described by a tuple (PRD, M_{OP}) , where

- $PRD = [\phi_1[prd_1], \dots, \phi_K[prd_K]]$ is the production sequence with ϕ phases, where $\phi = \sum_{i=1}^K \phi_i$ is determined by the mapping relation M in Definition 2, and $prd_1, \dots, prd_K \in \mathbb{N}$.
- $M_{OP} : \vec{p}_i \rightarrow \psi_{OP}$ is mapping relation, where $\vec{p}_i \in \Pi$ and

$$\psi_{OP} = \{\phi_1, \dots, \phi_K, prd_1, \dots, prd_K\}. \quad (6)$$

The consumption/production sequence defined here is a generalization of that for the CSDF MoC (see Section III-B). We can see that a CSDF actor has a constant ϕ phases in its consumption/production sequences, whereas the length of the phase of an MADF actor is parameterized by $\phi = \sum_{i=1}^K \phi_i$. In addition, the mapping relation M_{IP}/M_{OP} must be provided by the application designer. Consider the two input ports IP_1 and IP_2 of actor A_5 in Fig. 1. The mapping relations M_{IP_1} and M_{IP_2} are represented as follows:

$$M_{IP_1} : \vec{p}_5 = [p_5, p_6] \rightarrow \psi_{IP_1} = \{\phi_1, \phi_2, cns_1, cns_2\} = \{1, 1, p_5, 0\}, \quad (7)$$

$$M_{IP_2} : \vec{p}_5 = [p_5, p_6] \rightarrow \psi_{IP_2} = \{\phi_1, \phi_2, cns_1, cns_2\} = \{1, 1, 0, p_6\}. \quad (8)$$

It can be seen that parameter p_5 is mapped to cns_1 of IP_1 , parameter p_6 is mapped to cns_2 of IP_2 , and ϕ_1 and ϕ_2 both are constant equal to 1. Therefore, the consumption sequence of IP_1 is $CNS = [1[p_5], 1[0]] = [p_5, 0]$ and the consumption sequence of IP_2 is $CNS = [1[0], 1[p_6]] = [0, p_6]$. Similarly considering output port OP_1 of actor A_4 , its mapping relation M_{OP_1} is given as:

$$M_{OP_1} : \vec{p}_4 = [p_4] \rightarrow \psi_{OP_1} = \{\phi_1, prd_1\} = \{1, p_4\}. \quad (9)$$

In this case, parameter p_4 is mapped to prd_1 and $\phi_1 = 1$. Therefore, production sequence $PRD = [1[p_4]] = [p_4]$ is obtained for OP_1 of A_4 .

Definition 6 (Edge). An edge $E \in \mathcal{E}$ is defined by a tuple $((A_i, OP), (A_j, IP))$, where

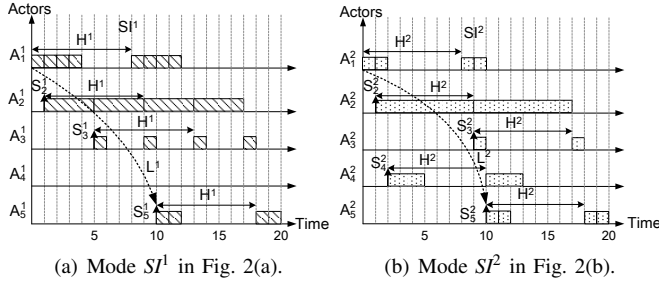


Fig. 3. Execution of two iterations of both modes SI^1 and SI^2 under self-timed scheduling.

- actor A_i produces a parameterized number of tokens to edge E through output port OP ;
- actor A_j consumes a parameterized number of tokens from E through input port IP .

Considering edge E_5 in Fig. 1, it connects output port OP_1 of actor A_4 to input port IP_2 of actor A_5 .

Definition 7 (Mode of MADF). A mode SI^i of MADF is a consistent and live CSDF graph, denoted as G^i , obtained by setting values of Π in Definition 1 as follows:

$$\forall \vec{p}_k \in \Pi : \vec{p}_k = MC_k(SI^i), \quad (10)$$

where function MC_k is given in Definition 3.

Definition 8 (Mode of MADF Actor). An actor A_k in mode SI^i , denoted by A_k^i , is a CSDF actor obtained from A_k as follows:

$$\vec{p}_k = MC_k(SI^i). \quad (11)$$

Fig. 2(a) shows the CSDF graph of mode SI^1 and Fig. 2(b) shows the CSDF graph of mode SI^2 . Consider function MC_5 for actor A_5 in Table II with parameter vector $\vec{p}_5 = [p_5, p_6]$. For instance, mode SI^1 results in $\vec{p}_5 = [p_5, p_6] = [2, 0]$, where parameter values $p_5 = 2$ and $p_6 = 0$. Consequently, according to mapping relations M_{IP_1} and M_{IP_2} given in Equation (7) and Equation (8), $cn_{s_1} = p_5 = 2$ can be obtained for input port IP_1 and $cn_{s_2} = p_6 = 0$ for IP_2 . This determines actor A_5^1 shown in Fig. 2(a) for mode SI^1 .

Definition 9 (Inactive Actor). A MADF actor A_i^k is inactive in mode SI^k if the following conditions hold:

- 1) $\forall IP \in \mathcal{I}_i : CNS = [0, \dots, 0]$;
- 2) $\forall OP \in \mathcal{O}_i : PRD = [0, \dots, 0]$.

Otherwise, A_i^k is called active in mode SI^k .

For actor A_4^1 shown in Fig. 2(a), it has consumption and production sequence $[0]$. Therefore, actor A_4 is said to be inactive in mode SI^1 .

B. Operational Semantics

During execution of a MADF graph, it can be either in a steady-state or mode transition.

Definition 10 (Steady-state). A MADF graph is in a steady-state of a mode SI^i , if it satisfies Equation (10) with the same SI^i for all its actors.

TABLE III
ACTOR PARAMETER FOR G_1 IN FIG. 1.

Mode	SI^1				SI^2				
Actor	A_1^1	A_2^1	A_3^1	A_5^1	A_1^2	A_2^2	A_3^2	A_4^2	A_5^2
WCET (μ_i)	1	4	1	1	1	8	1	3	1
period (T_i)	2	4	4	4	4	8	8	8	4
starting time (S_i)	0	2	6	14	0	4	12	8	20
utilization (u_i)	$\frac{1}{2}$	1	$\frac{1}{4}$	$\frac{1}{4}$	$\frac{1}{4}$	1	$\frac{1}{8}$	$\frac{3}{8}$	$\frac{1}{4}$

Definition 11 (Mode Transition). A MADF graph is in a mode transition from mode SI^o to SI^l , where $o \neq l$, if some actors have SI^o for Equation (11) and the remaining active actors have SI^l for Equation (11).

In the steady-state of a MADF graph, all active actors execute in the same mode. As defined previously in Definition 7 and shown in Fig. 2(a) and Fig. 2(b), the steady-state of the MADF graph has the same operational semantics as a CSDF graph. We use $\langle A_i^k, x \rangle$ to denote the x -th firing of actor A_i in mode SI^k . At $\langle A_i^k, x \rangle$, it executes computation $\bar{C}_i((x-1) \bmod \phi + 1)$, where \bar{C}_i is given in Definition 2. The number of tokens consumed and produced are specified according to Definitions 4 and 5, respectively. For instance, the x -th firing of A_i^k produces $PRD((x-1) \bmod \phi + 1)$ tokens through an output port OP . In each mode SI^k , the MADF graph is a consistent and live CSDF graph and thus has the notion of graph iterations with a non-trivial repetition vector $\vec{q}^k \in \mathbb{N}^{|\mathcal{A}|}$ resulting from Equation (1). Next, we further define mode iterations.

Definition 12 (Mode Iteration). One iteration It^k of a MADF graph in mode SI^k consists of one firing of control actor A_c and $q_i^k \in \vec{q}^k$ firings of each MADF actor A_i^k .

Consider the two modes shown in Fig. 2(a) and Fig. 2(b). Repetition vectors \vec{q}^1 and \vec{q}^2 are:

$$\vec{q}^1 = [4, 2, 2, 0, 2], \quad \vec{q}^2 = [2, 1, 1, 1, 2]. \quad (12)$$

For any mode of a MADF graph, i.e., a live CSDF graph, under any valid schedule, it has (eventually) periodic execution in time. This holds for CSDF graphs under self-timed schedule [17], K-periodic schedule [18], and SPS [14]. The length of the periodic execution, called *iteration period*, determines the minimum time interval to complete one graph iteration (cf. Definition 12). The iteration period, denoted by H^k , is equal for any actor in the same mode SI^k . During a periodic execution, the starting time of each actor A_i^k , denoted by S_i^k , indicates the time distance between the start of source actor A_{src}^k and the start of actor A_i^k in the same iteration period. Based on the notion of starting times, we define *iteration latency* L^k of a MADF graph in mode SI^k as follows:

$$L^k = S_{snk}^k - S_{src}^k, \quad (13)$$

where S_{snk}^k and S_{src}^k are the earliest starting times of the sink and source actors, respectively. Fig. 3 illustrates the execution of both modes SI^1 and SI^2 given in Fig. 2 under the self-timed schedule. A rectangle denotes the WCET of an actor firing. The WCETs of all actors in both modes are given in the third row of Table III. Now, it can be seen in Fig. 3 that iteration period $H^1 = H^2 = 8$. Based on the starting time of each actor,

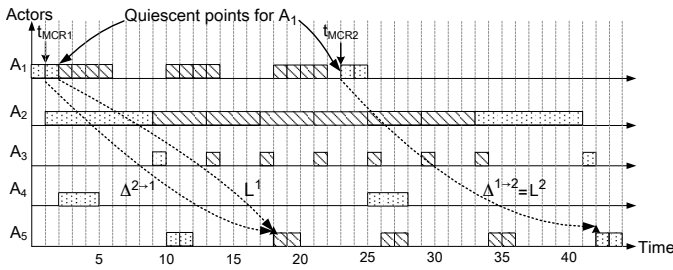


Fig. 4. An execution of G_1 in Fig. 1 with two mode transitions under the ST transition protocol. $MCR1$ at time t_{MCR1} denotes a transition request from mode S^2 to S^1 , and $MCR2$ at time t_{MCR2} denotes a transition request from mode S^1 to S^2 .

we obtain iteration latencies $L^1 = S_5^1 - S_1^1 = 10 - 0 = 10$ and $L^2 = S_5^2 - S_1^2 = 10 - 0 = 10$ as shown in Fig. 3.

C. Mode Transition

While the operational semantics of a MADF graph in steady-state are the same as that of a CSDF graph, the transition of MADF graph from one mode to another is the crucial part that makes it fundamentally different from CSDF. The protocol for mode transitions has strong impact on the compile-time analyzability and implementation efficiency. In this section, we propose a novel and efficient protocol of mode transitions for MADF graphs.

During execution of a MADF graph, mode transitions may be triggered at run-time by receiving a Mode Change Request (MCR) from the external environment. We first assume that a MCR can be only accepted in the steady-state of a MADF graph, not in an ongoing mode transition. This means that any MCR occurred during an ongoing mode transition will be ignored. Consider a mode transition from S^o to S^l . The transition is accomplished by the control actor reading mode identifier S^l from its control input port (see the black dot in Fig. 1) and writing parameter values of \vec{p}_i to the control output port connected to each dataflow actor A_i^l according to function MC_i given in Definition 3. Then, A_i^l reads new parameter values \vec{p}_i from its control input port and sets the sequence of computations according to mapping relation M_i in Definition 2. The production and consumption sequences are obtained in accordance with M_{IP} and M_{OP} in Definition 4 and Definition 5, respectively. We further define/require that mode transitions are only allowed at quiescent points [19].

Definition 13 (Quiescent Point of MADF). *For mode S^l , a quiescent point of MADF actor A_i is firing $\langle A_i^l, x \rangle$ in mode iteration I^l that satisfies*

$$\neg \exists \langle A_i^l, y \rangle \in I^l : y < x. \quad (14)$$

Definition 13 simply refers to the first firing of actor A_i in each iteration I^l of mode S^l . Recall that each iteration of mode S^l consists of q_i^l firings of actor A_i . Therefore, our requirement that a mode transition is only allowed at a quiescent point implies that a transition from mode S^l to S^o of actor A_i happens when all firings of actor A_i are completed in the iteration of S^l when MCR occurs. Fig. 4 shows an execution of G_1 in Fig. 1 with two mode transitions. For instance, the

MCR at time $t_{MCR1} = 1$ denotes a transition request from mode S^2 to S^1 . The mode transition of actor A_1 happens when all firings of actor A_1 are completed, that is at time 2 in Fig. 4 in this particular example.

Definition 13 defines mode transitions of MADF graphs as partially ordered actor firings. However, it does not specify at which time instance a mode transition actually starts. Therefore, below, we focus on the transition protocol that defines the points in time for occurrences of mode transitions. To quantify the transition protocol, we introduce a metric, called *transition delay*, to measure the responsiveness of a protocol to a MCR.

Definition 14 (Transition Delay). *For a MCR at time t_{MCR} calling for a mode transition from mode S^o to S^l , the transition delay $\Delta^{o \rightarrow l}$ of a MADF graph is defined as*

$$\Delta^{o \rightarrow l} = \sigma_{snk}^{o \rightarrow l} - t_{MCR}, \quad (15)$$

where $\sigma_{snk}^{o \rightarrow l}$ is the earliest starting time of the sink actor in the new mode S^l .

In Fig. 4, we can compute the transition delay for $MCR1$ occurred at time $t_{MCR1} = 1$ as $\Delta^{2 \rightarrow 1} = 18 - 1 = 17$.

1) *Self-timed Transition Protocol*: In the existing adaptive MoCs like FSM-SADF [5], a protocol, referred here as *Self-Timed* (ST) transition protocol, is adopted. The ST protocol specifies that actors are scheduled in the self-timed manner not only in the steady-state, but also during a mode transition. For FSM-SADF upon a MCR, a firing of a FSM-SADF actor in the new mode can start immediately after the firing of the actor completes the old mode iteration. The only possible delay is introduced due to availability of input data. One reason behind the ST protocol is that the ST schedule for a (C)SDF graph (steady-state of FSM-SADF¹) leads to its highest achievable throughput. However, the ST protocol generally introduces interference of one mode execution with another one. The time needed to complete mode transitions also fluctuates as the transition delay of an ongoing transition depends on the transitions that occurred in the past. We consider this as an undesired effect because mode transitions using the ST protocol become potentially slow and unpredictable. Another consequence of the incurred interference between modes using the ST transition protocol is the high time complexity of analyzing transition delays, because transition delays cannot be analyzed independently for each mode transition. The analysis proposed in [5] uses an approach based on state-space exploration, which has the exponential time complexity.

Consider G_1 in Fig. 1 and an execution of G_1 with the two mode transitions illustrated in Fig. 4. The execution is assumed under the ST schedule for both steady-state and mode transitions of G_1 . After $MCR1$ at time t_{MCR1} , the transition from mode S^2 to S^1 introduces interference to execution of the new mode S^1 from execution of the old mode S^2 . The interference increases the iteration latency of the new mode S^1 to $L^1 = S_5^1 - S_1^1 = 18 - 2 = 16$ from initially 10 as shown in Fig. 3(a) when G_1 is only executed in the steady-state of

¹The steady-state of SADF is defined similarly to that of MADF. The only difference is that a scenario of FSM-SADF is a SDF graph, whereas a mode of MADF is a CSDF graph.

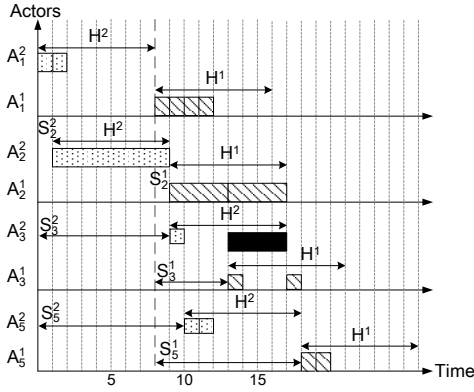


Fig. 5. An illustration of the Maximum-Overlap Offset (MOO) calculation.

mode SI^1 . Even worse, the interference is further propagated to the second mode transition after $MCR2$ at time t_{MCR2} . In this case, the iteration latency $L^2 = S_5^2 - S_1^2 = 42 - 23 = 19$ is increased from initially 10 as shown in Fig. 3(b) when G_1 is only executed in the steady-state of mode SI^2 . This example thus clearly shows the problem of the ST protocol. That is, it introduces interference between the old and new modes due to mode transitions, thereby increasing the iteration latency of the new mode in the steady-state after the transition. Furthermore, the increase of iteration latency also potentially increases transition delays as it will be shown in the next section.

2) *Maximum-Overlap Offset Transition Protocol*: To address the problem of the ST transition protocol explained above, we propose a new transition protocol, called *Maximum-Overlap Offset (MOO)*.

Definition 15 (Maximum-Overlap Offset (MOO)). *For a MADF graph and a transition from mode SI^o to SI^l , Maximum-Overlap Offset (MOO), denoted by x , is defined as*

$$x = \begin{cases} \max_{A_i \in \mathcal{A}^o \cap \mathcal{A}^l} (S_i^o - S_i^l) & \text{if } \max_{A_i \in \mathcal{A}^o \cap \mathcal{A}^l} (S_i^o - S_i^l) > 0 \\ 0 & \text{otherwise,} \end{cases} \quad (16)$$

where $\mathcal{A}^o \cap \mathcal{A}^l$ is set of actors active in both modes SI^o and SI^l .

Basically, we first assume that the new mode SI^l starts immediately after the source actor A_{src}^o of the old mode SI^o completes its last iteration I^o . All actors A_i^l of the new mode execute according to the earliest starting times S_i^l and iteration period H^l in the steady-state. Under this assumption, if the execution of the new mode overlaps with the execution of the old mode in terms of iteration periods H^o and H^l , we then need to offset the starting time of the new mode by the maximum overlap among all actors. In this way, the execution of the new mode will have the same iteration latency as that of the new mode in the steady-state, i.e., no interference between the execution of both old and new modes.

Consider $MCR1$ at time t_{MCR1} shown in Fig. 4. Obtaining MOO x is illustrated in Fig. 5. We first assume that the new mode SI^1 starts at the time when the source actor A_1^2 completes the last iteration at time 8 (see bold, dashed line in Fig. 5). Actors A_i^1 in the new mode start as if they executed in the

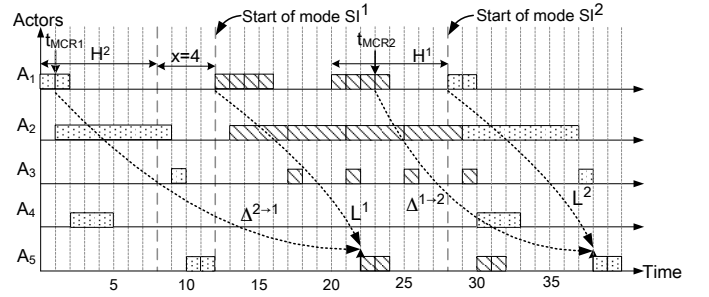


Fig. 6. The execution of G_1 with two mode transitions under Maximum-Overlap Offset (MOO) protocol.

steady-state of mode SI^1 . Then, we can see that, for actor A_3 , the execution of A_3^1 in the new mode SI^1 according to S_3^1 in Fig. 3(a) overlaps 4 time units (solid bar in Fig. 5) with the execution of A_3^2 in the old mode SI^2 in terms of iteration periods H^2 and H^1 . This is also the maximum overlap between the execution of actors in modes SI^2 and SI^1 . According to Definition 15, x can be obtained through the following equations:

$$\begin{aligned} S_1^2 - S_1^1 &= 0 - 0 = 0, & S_2^2 - S_2^1 &= 1 - 1 = 0, \\ S_3^2 - S_3^1 &= 9 - 5 = 4, & S_5^2 - S_5^1 &= 10 - 10 = 0. \end{aligned}$$

Therefore, it results in an offset $x = \max(0, 0, 4, 0) = 4$ to the start of mode SI^1 and is shown in Fig. 6. The starting time of the new mode SI^1 , namely the source actor A_1^1 , must be first delayed to the time when A_2^1 completes the iteration period H^2 in the last iteration, namely time 8 shown as the first bold dashed line in Fig. 6. In addition, the MOO $x = 4$ must be further added to the starting time of A_1^1 (the second bold dashed line in Fig. 6). Fig. 6 also shows another transition from mode SI^1 to SI^2 with a MCR occurred at time $t_{MCR2} = 23$. The starting time of the source actor A_1^2 in the new mode SI^2 must be first delayed to the time 28 (the third bold dashed line in Fig. 6), namely the time when A_1^1 completes the last iteration in the old mode SI^1 . To calculate the MOO x for this transition, the following equations hold:

$$\begin{aligned} S_1^1 - S_1^2 &= 0 - 0 = 0, & S_2^1 - S_2^2 &= 1 - 1 = 0, \\ S_3^1 - S_3^2 &= 5 - 9 = -4, & S_5^1 - S_5^2 &= 10 - 10 = 0. \end{aligned}$$

Thus, the equations above result in $x = \max(0, 0, -4, 0) = 0$. For this transition, the new mode SI^2 starts at time 28 as shown in Fig. 6.

The MOO protocol offers several advantages over the ST protocol. Essentially, the MOO protocol retains the iteration latency of the MADF graph in the new mode the same as the initial value, thereby avoiding the interference between the old and new modes. For instance, after $MCR1$ and $MCR2$ in Fig. 6, mode SI^1 and SI^2 still have the initial iteration latency $L^1 = 10$ and $L^2 = 10$ as shown in Fig. 3. Therefore, efficiently computing the starting time of MADF actors in the new mode becomes feasible and it plays an important role in deriving a hard-real time schedule for the MADF actors. As a result, analysis of the worst-case transition delay is much simpler (see Theorem 2) than that of the ST protocol, because the transition delay does not depend on the order of the transitions that occurred previously.

Concerning the transition delay, it may be the case that the MOO protocol results in initially longer transition delay than the ST protocol does due to the offset given in Definition 15. For $MCR1$ occurred at time t_{MCR1} , the transition delay of the MOO protocol is $\Delta^{2 \rightarrow 1} = 22 - 1 = 21$ as shown in Fig. 6, whereas the transition delay of the ST protocol is equal to $\Delta^{2 \rightarrow 1} = 18 - 1 = 17$ as shown in Fig. 4. On the other hand, let us consider the same transition request $MCR2$ occurred at time $t_{MCR2} = 23$ shown in Fig. 4 and Fig. 6. For $MCR2$, the ST protocol results in transition delay $\Delta^{1 \rightarrow 2} = 42 - 23 = 19$ as shown in Fig. 4. In contrast, the transition delay for the MOO protocol is $\Delta^{1 \rightarrow 2} = 38 - 23 = 16$ as shown in Fig. 6. The MOO protocol could provide shorter transition delay than the ST protocol, thereby faster responsiveness to a mode transition.

V. HARD REAL-TIME ANALYSIS AND SCHEDULING OF MADF

Based on the proposed MOO protocol for mode transitions, in this section, we propose a hard real-time analysis and scheduling framework for MADF. More specifically, we propose an analysis technique for mode transitions in MADF to reason about transition delays, such that timing constraints can be guaranteed. The hard real-time scheduling framework for MADF graphs is an extension of the SPS [14] framework initially developed for CSDF graphs.

As explained in Section III-C, the key concept of the SPS framework is to derive a periodic taskset representation for a CSDF graph. Since the steady-state of a mode can be considered as a CSDF graph according to Definitions 7 and 10, it is thus straightforward to represent the steady-state of a MADF graph as a periodic taskset and schedule the resulting taskset using any well-known hard real-time scheduling algorithm. Using the SPS framework, we can derive the two main parameters for each MADF actor in mode SI^k , namely the period (T_i^k in Equation (2)) and the earliest starting time (S_i^k in Equation (3)). Under SPS, the iteration period in mode SI^k is obtained as $H^k = q_i^k T_i^k$, $\exists A_i^k \in \mathcal{A}$. Below, we focus on determining the earliest starting time of each actor in the new mode upon a transition. From the earliest starting time, we can reason about the transition delay to quantify the responsiveness of a transition.

Upon a MCR, a MADF graph can safely switch to the new mode if all of its actors have completed their last iteration in the old mode upon synchronous protocol. In this case, the firings of MADF actors in the new mode do not overlap with the firings of actors in the old mode. This is called synchronous protocol [12] in real-time systems with mode change. One of its advantages is the simplicity, i.e., the synchronous protocol does not require any schedulability test at both compile-time and run-time. However, other protocols lead to earlier starting times than the synchronous protocol. Therefore, the synchronous protocol sets an upper bound on the earliest starting time for each MADF actor in the new mode.

Lemma 1. *For a MADF graph G under SPS and a MCR from mode SI^o to SI^l at time t_{MCR} , the earliest starting time of actor A_i^l , $\hat{\sigma}_i^{o \rightarrow l}$, is upper bounded by*

$$\hat{\sigma}_i^{o \rightarrow l} = F_{src}^o + S_{snk}^o + S_i^l, \quad (17)$$

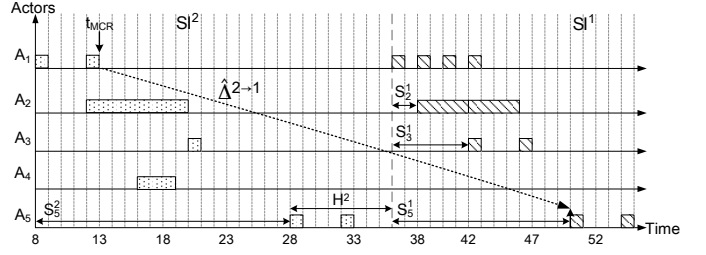


Fig. 7. Upper bounds of earliest starting times for transition from mode SI^2 to SI^1 .

where F_{src}^o indicates the time when the source actor A_{src}^o completes its last iteration It^o of the old mode SI^o and is given by

$$F_{src}^o = t_S^o + \left\lceil \frac{t_{MCR} - t_S^o}{H^o} \right\rceil H^o. \quad (18)$$

t_S^o is the starting time of mode SI^o and H^o is the iteration period of mode SI^o .

Proof. As explained previously for a transition from mode SI^o to SI^l , the upper bound of the earliest starting time for each actor A_i^l is computed in such a way that no firings of actors A_i^o and A_i^l occur simultaneously. This means, the start of an actor A_i^l must be later than all actors A_i^o have completed the last iteration It^o of the old mode SI^o . Given that mode SI^o starts at time t_S^o , the completion time of all actors A_i^o in the last iteration It^o can be thus computed as

$$F_{snk}^o = t_S^o + \left\lceil \frac{t_{MCR} - t_S^o}{H^o} \right\rceil H^o + S_{snk}^o + H^o. \quad (19)$$

where F_{snk}^o is the time when the old mode SI^o completes the last iteration It^o . It is assumed that the sink actor A_{snk}^o is the last actor to complete the iteration, i.e., $\forall A_i^o \in \mathcal{A}, S_i^o \leq S_{snk}^o$. Given Equation (18), Equation (19) can be rewritten as

$$F_{snk}^o = t_S^o + \left\lceil \frac{t_{MCR} - t_S^o}{H^o} \right\rceil H^o + S_{snk}^o = F_{src}^o + S_{snk}^o.$$

Now, starting the source actor A_{src}^l at any time later than F_{snk}^o is valid without introducing simultaneous execution of actors A_i^o and A_i^l . Therefore, the earliest starting time of source actor A_{src}^l is $\hat{\sigma}_{src}^{o \rightarrow l} = F_{snk}^o$. For any actor $A_i^l \in \mathcal{A} \setminus A_{src}^l$, its earliest starting times must satisfy Equation (3) imposed by the SPS framework. That is, the earliest starting time $\hat{\sigma}_i^{o \rightarrow l}$ of actor A_i^l can be obtained by adding S_i^l to $\hat{\sigma}_{src}^{o \rightarrow l}$. \square

Let us consider the actor parameters given in Table III for G_1 in Fig. 1. The third row shows the WCET for each actor in modes SI^1 and SI^2 . Based on WCETs, the period (fourth row in Table III) and the earliest starting time (fifth row in Table III) for each actor in the steady-state of both modes are obtained according to Equation (2) and Equation (3), respectively. Given \bar{q}^2 in Equation (12), we can also compute iteration period $H^2 = q_1^2 T_1^2 = 2 \times 4 = 8$. Now consider the mode transition from mode SI^2 to SI^1 shown in Fig. 7. Assume that the MCR occurs at time $t_{MCR} = 13$ and mode SI^2 starts at time $t_S^2 = 8$. The completion time of the last iteration It^2 is equal to the completion time of the sink actor A_5^2 computed as

$$F_{snk}^2 = t_S^2 + \left\lceil \frac{t_{MCR} - t_S^2}{H^2} \right\rceil H^2 + S_5^2 = 8 + \left\lceil \frac{13 - 8}{8} \right\rceil 8 + 20 = 36.$$

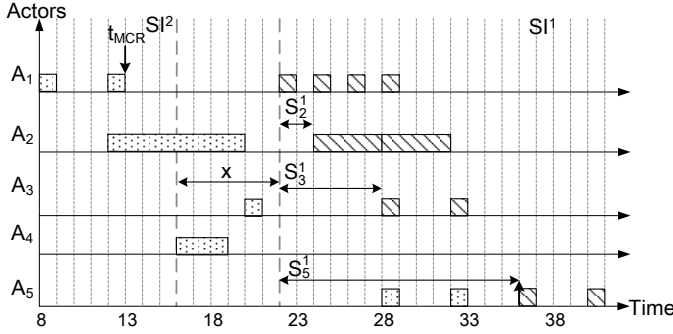


Fig. 8. Earliest starting times for transition from mode S^2 to S^1 with the MOO protocol.

In Fig. 7, F_{src}^2 corresponds to the earliest starting time of the source actor A_1^1 (bold dashed line). Finally, we can compute the earliest starting time for each actor in the new mode S^1 by adding S_i^1 . Considering for instance the sink actor A_5^1 in the new mode with $S_5^1 = 14$, the upper bound of its earliest starting time can be obtained as

$$\hat{\sigma}_5^{2 \rightarrow 1} = F_{\text{src}}^2 + S_5^2 + S_5^1 = F_{\text{src}}^2 + S_5^1 = 36 + 14 = 50.$$

We can thus compute the transition delay (cf. Definition 14) as

$$\hat{\Delta}^{2 \rightarrow 1} = \hat{\sigma}_5^{2 \rightarrow 1} - t_{\text{MCR}} = 50 - 13 = 37.$$

Although the upper bound of the earliest starting times is easy to obtain for MADF actors in the new mode, it does not provide a responsive mode transition. Therefore, here we aim at deriving a lower bound of the earliest starting times with the proposed MOO protocol.

Lemma 2. For a MADF graph under SPS and a MCR from mode S^p to S^l at time t_{MCR} , the earliest starting time of actor A_i^l using the MOO protocol is lower bounded by $\check{\sigma}_i^{p \rightarrow l}$ given as

$$\check{\sigma}_i^{p \rightarrow l} = F_{\text{src}}^o + x + S_i^l, \quad (20)$$

where F_{src}^o is given in Equation (18) and x is given in Equation (16).

Proof. Under the MOO protocol, the start of actor A_i^l must be later than the time when A_i^o , if any, completes its last iteration in the old mode S^p . We assume that the source actor A_{src}^l is the first actor to start in the new mode S^l , i.e., $\forall A_i^l \in \mathcal{A}, S_i^l \geq S_{\text{src}}^l$. Thus, the starting time of the source actor A_{src}^l is at least equal to the completion time of the last iteration of A_{src}^o , denoted by F_{src}^o . Given F_{src}^o in Equation (18), it thus holds $\check{\sigma}_{\text{src}}^{p \rightarrow l} \geq F_{\text{src}}^o$. Then, the offset x because of the MOO protocol given in Equation (16) must be taken into account. Consequently, the earliest starting time of A_{src}^l is lower bounded by $\check{\sigma}_{\text{src}}^{p \rightarrow l} = F_{\text{src}}^o + x$. For any actor $A_i^l \in \mathcal{A} \setminus A_{\text{src}}^l$, its earliest starting times must satisfy Equation (3) imposed by the SPS framework. Hence, the earliest starting time $\check{\sigma}_i^{p \rightarrow l}$ of actor A_i^l can be obtained by adding S_i^l to $\check{\sigma}_{\text{src}}^{p \rightarrow l}$. \square

Let us consider again the transition from mode S^2 to S^1 . With the MOO protocol, the mode transition is illustrated in Fig. 8. Upon the MCR at time $t_{\text{MCR}} = 13$ and $t_S^2 = 8$, source

actor A_1^2 completes its last iteration I^2 in the old mode S^2 at the time (cf. Equation (18)) given as

$$F_{\text{src}}^2 = F_1^2 = t_S^2 + \left\lceil \frac{t_{\text{MCR}} - t_S^2}{H^2} \right\rceil H^2 = 8 + \left\lceil \frac{13 - 8}{8} \right\rceil 8 = 16.$$

This is the earliest possible time at which mode transition is allowed. For MOO, x can be computed according to Equation (16). Therefore, the following equations hold:

$$\begin{aligned} S_1^2 - S_1^1 &= 0 - 0 = 0, & S_2^2 - S_2^1 &= 4 - 2 = 2, \\ S_3^2 - S_3^1 &= 12 - 6 = 6, & S_5^2 - S_5^1 &= 20 - 14 = 6. \end{aligned}$$

It thus yields $x = \max(0, 2, 6, 6) = 6$, i.e., an offset $x = 6$ is added to F_{src}^2 . It can be seen in Fig. 8 that the source actor A_1^1 starts at time $F_{\text{src}}^2 + x = 16 + 6 = 22$. Finally, the earliest starting times of actors in mode S^1 can be determined by adding S_i^1 . Considering for instance A_5^1 in the new mode, the lower bound of its earliest starting time can be obtained as:

$$\check{\sigma}_5^{2 \rightarrow 1} = F_{\text{src}}^2 + x + S_5^1 = 16 + 6 + 14 = 36.$$

Now, the transition delay (cf. Definition 14) can be obtained as

$$\check{\Delta}^{2 \rightarrow 1} = \check{\sigma}_5^{2 \rightarrow 1} - t_{\text{MCR}} = 36 - 13 = 23.$$

A. Scheduling Analysis under a Fixed Allocation of Actors

During a mode transition of a MADF graph according to the MOO protocol, actors execute simultaneously in the old and new modes. The derived starting time in Lemma 2 for each actor is only the lower bound because the allocation of actors on PEs is not taken into account yet. That means, the derived starting times according to Lemma 2 can be only achieved during mode transitions when each actor is allocated to a separate PE. In a practical system where multiple actors are allocated to the same PE, the PE may be potentially overloaded during mode transitions. To avoid overloading of PEs, the earliest starting times of actors may be further delayed.

Lemma 3. For a MADF graph under SPS, a MCR from mode S^p to S^l , and a m -partition of all actors $\Psi = \{\Psi_1, \dots, \Psi_m\}$, where m is the number of PEs, the earliest starting time of an actor A_i^l without overloading the underlying PE is given by

$$\sigma_i^{p \rightarrow l} = F_{\text{src}}^o + \delta^{p \rightarrow l} + S_i^l, \quad (21)$$

where F_{src}^o is computed by Equation (18) and $\delta^{p \rightarrow l}$ is obtained as

$$\delta^{p \rightarrow l} = \min_{t \in [x, S_{\text{src}}^o]} \{t : U_j(k) \leq UB, \forall k \in [t, S_{\text{src}}^o] \wedge \forall \Psi_j \in \Psi\}. \quad (22)$$

UB denotes the utilization bound of the scheduling algorithm used to schedule actors on each PE. Ψ_j contains the set of actors allocated to PE $_j$. $U_j(k)$ is the total utilization of PE $_j$ at time k demanded by both mode S^p and S^l actors, and is given by

$$U_j(k) = \underbrace{\sum_{A_d^o \in \Psi_j} (u_d^o - h(k - S_d^o) \cdot u_d^o)}_{U_j^o(k)} + \underbrace{\sum_{A_d^l \in \Psi_j} (h(k - S_d^l - t) \cdot u_d^l)}_{U_j^l(k)}, \quad (23)$$

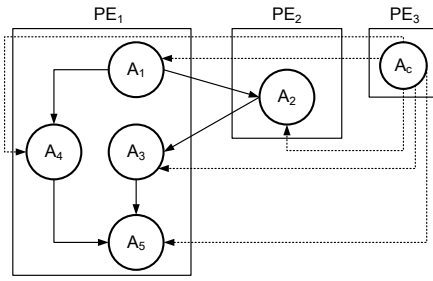


Fig. 9. Allocation of all MADF actors in Fig. 1 to 3 PEs.

$A_d^o \in \Psi_j$ is an actor active in the old mode SI^o and allocated to PE_j . $A_d^l \in \Psi_j$ is an actor active in the new mode SI^l and allocated to PE_j . $h(t)$ is the Heaviside step function.

Proof. Lemma 2 shows the lower bound of the earliest starting time for actor A_i^l in the new mode SI^l . However, starting A_i^l at time $\delta_i^{o \rightarrow l}$ may overload PE_j , i.e., the resulting total utilization of PE_j , denoted by $U_j(\delta_i^{o \rightarrow l})$, exceeds UB . Therefore, in this case, the earliest starting time $\delta_i^{o \rightarrow l}$ must be delayed by $\delta^{o \rightarrow l}$ such that $U_j(\delta_i^{o \rightarrow l}) \leq UB$ holds. From Equation (21) and Equation (20), we can see that $\delta^{o \rightarrow l}$ is lower bounded by x which corresponds to the MOO protocol. In addition, $\delta^{o \rightarrow l}$ is upper bounded by S_{snk}^o if we consider Equation (21) and Equation (17).

$\delta^{o \rightarrow l}$ of interest is the minimum time t in the bounded interval $[x, S_{snk}^o]$ that satisfies two conditions.

Condition 1: For each PE_j , the total utilization cannot exceed UB at time t , i.e., $U_j(t) \leq UB$. The total utilization $U_j(t)$ in Equation (23) consists of two parts, namely $U_j^o(t)$ and $U_j^l(t)$. $U_j^o(t)$ denotes the PE capacity occupied by the actors in mode SI^o that are not completed yet. Additional PE capacity $U_j^l(t)$ is demanded by the already released actors in the new mode SI^l .

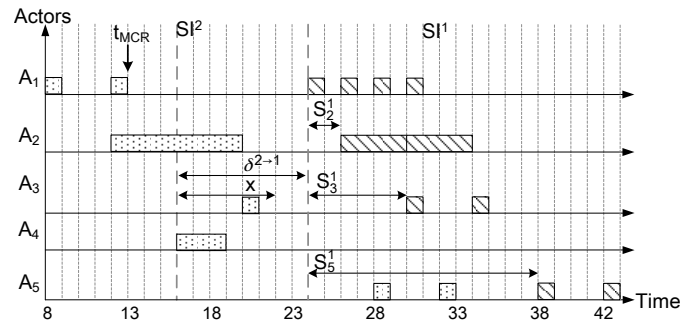
Condition 2: We need to check all time instants $k > t$ in the interval $[t, S_{snk}^o]$, such that $U_j(k) \leq UB$, to guarantee that each PE_j is not overloaded during the mode transition. \square

Fig. 9 shows all actors of G_1 in Fig. 1 allocated to 3 PEs and let us assume that the actors allocated to each PE are scheduled using the EDF scheduling algorithm [16]. The utilization bound of EDF is given in [16] as $UB = 1$. Given this allocation and the transition from mode SI^2 to SI^1 shown in Fig. 8, the lower bound of the earliest starting time $\delta_1^{2 \rightarrow 1} = 22$ for actor A_1^1 cannot be achieved. At time 22, only actor A_1^2 has completed the last iteration It^2 on PE_1 . Starting the new mode SI^1 at time 22 corresponds to $\delta^{2 \rightarrow 1} = x = 6$. The total utilization of PE_1 demanded by the actors in the old mode SI^2 at time 22, i.e., $U_1^2(6)$, can be computed as follows:

$$\begin{aligned} U_1^2(6) &= \sum_{A_d^2 \in \Psi_1} u_d^2 - h(6 - S_d^2) \cdot u_d^2, \quad d \in \{1, 3, 4, 5\} \\ &= u_1^2 - h(6) \cdot u_1^2 + u_3^2 - h(-6) \cdot u_3^2 + u_4^2 - h(-2) \cdot u_4^2 + u_5^2 - h(-14) \cdot u_5^2 \\ &= 0 + u_3^2 + u_4^2 + u_5^2 = \frac{1}{8} + \frac{3}{8} + \frac{1}{4} = \frac{3}{4}. \end{aligned}$$

Enabling A_1^1 in the new mode SI^1 at time 22 would yield

$$U_1(6) = U_1^2(6) + u_1^1 = \frac{3}{4} + \frac{1}{2} > UB = 1,$$

Fig. 10. Earliest starting times for transition SI^2 to SI^1 on 3 PEs shown in Fig. 9.

thereby leading to being unschedulable on PE_1 . In this case, the earliest starting times of all actors in mode SI^1 must be delayed by $\delta^{2 \rightarrow 1} = 8$ to time 24 as shown in Fig. 10. At time 24, the total utilization demanded by mode SI^2 actors is

$$\begin{aligned} U_1^2(8) &= \sum_{A_d^2 \in \Psi_1} u_d^2 - h(8 - S_d^2) \cdot u_d^2, \quad d \in \{1, 3, 4, 5\} \\ &= u_1^2 - h(8) \cdot u_1^2 + u_3^2 - h(-4) \cdot u_3^2 + u_4^2 - h(0) \cdot u_4^2 + u_5^2 - h(-12) \cdot u_5^2 \\ &= 0 + u_3^2 + 0 + u_5^2 = \frac{1}{8} + \frac{1}{4} = \frac{3}{8}. \end{aligned}$$

Now, enabling A_1^1 in the new mode at time 24 results in the total utilization of PE_1 as

$$U_1(8) = U_1^2(8) + u_1^1 = \frac{3}{8} + \frac{1}{2} < 1.$$

Next, assuming that the new mode SI^1 starts at time 24, we need to check that the remaining actors in the new mode SI^1 , namely A_3^1 and A_5^1 , can start with S_3^1 and S_5^1 respectively without overloading PE_1 . For instance, enabling A_3^1 at time 24 results in starting time $\delta_3^{2 \rightarrow 1} = 24 + S_3^1 = 24 + 6 = 30$. At time 30, the total utilization of PE_1 can be obtained according to Equation (23) as follows:

$$\begin{aligned} U_1^2(8+6) &= \sum_{A_d^2 \in \Psi_1} u_d^2 - h(14 - S_d^2) \cdot u_d^2, \quad d \in \{1, 3, 4, 5\} \\ &= u_1^2 - h(14) \cdot u_1^2 + u_3^2 - h(2) \cdot u_3^2 + u_4^2 - h(6) \cdot u_4^2 + u_5^2 - h(-6) \cdot u_5^2 \\ &= 0 + 0 + 0 + u_5^2 = \frac{1}{4}, \end{aligned}$$

$$\begin{aligned} U_1^1(8+6) &= \sum_{A_d^1 \in \Psi_1} (h(14 - S_d^1 - 8) \cdot u_d^1), \quad d \in \{1, 3, 5\} \\ &= h(6)u_1^1 + h(0)u_3^1 + h(-8)u_5^1 = \frac{1}{2} + \frac{1}{4} = \frac{3}{4}, \end{aligned}$$

$$U_1(8+6) = U_1^2(8+6) + U_1^1(8+6) = 1 = UB.$$

Hence, actors A_5^2 , A_1^1 , and A_3^1 are schedulable on PE_1 using EDF. Similarly, starting A_5^1 at time $\delta_5^{2 \rightarrow 1} = 24 + S_5^1 = 38$ still keeps the resulting set of actors schedulable on PE_1 .

Using Lemma 3, we can quantify the maximum and minimum transition delays for any transition from mode SI^o to SI^l .

Theorem 2. For a MADF graph under SPS, a fixed allocation of all MADF actors $\Psi = \{\Psi_1, \dots, \Psi_m\}$ to m PEs, and a MCR from mode SI^o to SI^l , the minimum transition delay is given by

$$\Delta_{min}^{o \rightarrow l} = \delta^{o \rightarrow l} + S_{snk}^l \quad (24)$$

and the maximum transition delay is given by

$$\Delta_{max}^{o \rightarrow l} = \delta^{o \rightarrow l} + S_{snk}^l + H^o, \quad (25)$$

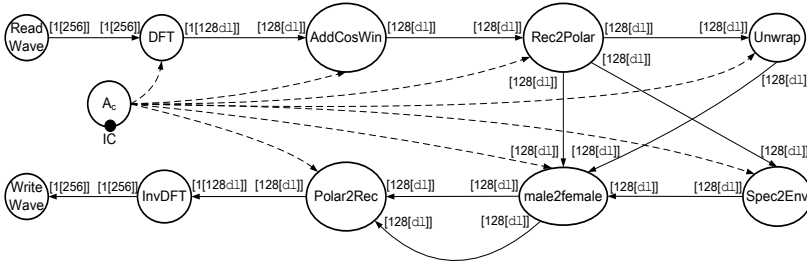


Fig. 11. MADF graph of Vocoder.

where $\delta^{o \rightarrow l}$ is computed by Lemma 3, S_{snk}^l is the starting time of the sink actor in the new mode SI^l , and H^o is the iteration period of the old mode SI^o .

Proof. For a MCR from mode SI^o to SI^l , the transition delay $\Delta^{o \rightarrow l}$ of a MADF graph is given in Definition 14 as $\Delta^{o \rightarrow l} = \sigma_{snk}^{o \rightarrow l} - t_{MCR}$, where the earliest starting time of the sink actor is calculated as $\sigma_{snk}^{o \rightarrow l} = F_{src}^o + \delta^{o \rightarrow l} + S_{snk}^l$ according to Lemma 3. Therefore, $\Delta^{o \rightarrow l}$ can be rewritten as $\Delta^{o \rightarrow l} = F_{src}^o + \delta^{o \rightarrow l} + S_{snk}^l - t_{MCR}$. Essentially, $\Delta^{o \rightarrow l}$ is composed of three parts. In the first part, the MOO transition protocol together with a fixed allocation of the MADF actors determine $\delta^{o \rightarrow l}$. The second part S_{snk}^l results from the SPS framework. These two parts thus can be determined at compile-time. The third part $F_{src}^o - t_{MCR}$ depends on when the MCR occurs, namely at t_{MCR} , which can only be determined at run-time. In the following, we distinguish two cases for t_{MCR} :

Case 1: Assume that the MCR occurs at the end of an iteration of the source actor in the old mode SI^o , i.e., $t_{MCR} = F_{src}^o$. Then, the source actor shall be only delayed by $\delta^{o \rightarrow l}$ to start in the new mode SI^l according to Lemma 3, thereby guaranteeing the fastest possible start of the new mode SI^l . As a consequence, it results in the minimum possible transition delay. Therefore, substituting $t_{MCR} = F_{src}^o$, we obtain

$$\Delta_{min}^{o \rightarrow l} = F_{src}^o + \delta^{o \rightarrow l} + S_{snk}^l - F_{src}^o = \delta^{o \rightarrow l} + S_{snk}^l.$$

Case 2: Assume that the MCR occurs at the beginning of an iteration of the source actor in the old mode SI^o , i.e., $t_{MCR} = F_{src}^o - H^o$. Then, the source actor cannot start in the new mode before it completes the whole iteration in the old mode SI^o followed by the delay $\delta^{o \rightarrow l}$ according to Lemma 3. Therefore, the maximum transition delay is computed as follows:

$$\Delta_{max}^{o \rightarrow l} = F_{src}^o + \delta^{o \rightarrow l} + S_{snk}^l - (F_{src}^o - H^o) = \delta^{o \rightarrow l} + S_{snk}^l + H^o.$$

□

It can be seen from Theorem 2 that the maximum and minimum transition delays solely depend on the allocation of MADF actors and the old and new modes in question, irrespective of the previously occurred transitions. The old and new modes determine H^o and S_{snk}^l , respectively, while the allocation of MADF actors determines the value of $\delta^{o \rightarrow l}$. Here, the offset x due to our MOO protocol is captured in $\delta^{o \rightarrow l}$ and can be considered as performance overhead if $x \neq 0$. The other parts, namely H^o and S_{snk}^l , in the maximum and minimum transition delays cannot be avoided as they will be present in any transition protocol.

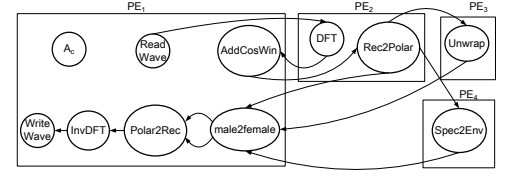


Fig. 12. Allocation of dataflow actors of Vocoder to 4 PEs. The control edges are omitted to avoid cluttering.

VI. CASE STUDIES

To evaluate our proposed MADF MoC and MOO protocol, in this section, we present two case studies. In the first case study, we model a real-life adaptive streaming application, called Vocoder, with our MADF MoC proposed in Section IV and apply the hard real-time analysis proposed in Section V. With this case study, we show that the MADF MoC is capable of capturing different application modes and the transitions between them. Then, in the second case study, we model another real-life adaptive streaming application, called MP3decoder, with MADF and we focus on analyzing the transition delays and demonstrating the effectiveness of our MADF model armed with the proposed MOO transition protocol compared to the well-known FSM-SADF model [5] which also can capture modes/scenarios. In this case study, we adopt self-timed scheduling for both our MADF and FSM-SADF models in the steady-state. The major difference between these models in this case study is their transition protocol which is the MOO protocol in our MADF model and the self-timed protocol in FSM-SADF. Another example of the application of our MOO protocol can be found in [20].

A. Case Study 1

In this section, we consider a real-life adaptive application from the StreamIT benchmark suit [21], called Vocoder, which implements a phase voice encoder and performs pitch transposition of recorded sounds from male to female. We modeled Vocoder using a MADF graph with 4 modes, which capture different workloads. The MADF graph of Vocoder is shown in Fig. 11. Depending on the desired quality of audio encoding and various performance requirements, the resource manager as a middle-ware or OS-like component for the MPSoC may switch between four different modes of Vocoder at run-time. The four modes $S = \{SI^8, SI^{16}, SI^{32}, SI^{64}\}$ specify different lengths of the Discrete Fourier Transform (DFT), denoted by dl $\in \{8, 16, 32, 64\}$. Mode SI^8 (dl = 8) requires the least amount of computation at the cost of the worst voice encoding quality among all DFT lengths. Mode SI^{64} (dl = 64) produces the best quality of voice encoding among all modes, but is computationally intensive. The other two modes SI^{16} and SI^{32} explore the trade-off between the quality of the encoding and computational workload. The resource manager, therefore, can take advantage of this trade-off and adjust the quality of the encoding according to the available resources, such as energy budget and number of PEs, at run-time. A transition

TABLE IV
WCETs of all actors in Vocoder (in clk. cycles).

Mode	ReadWave	DFT	AddCosWin	Rec2Polar	Unwrap	Spec2Env	male2female	Polar2Rec	InvDFT	WriteWave
SI^8	3704	16775	16	90	359	7168	1093	3	236	3660
SI^{16}	3704	35121	35	183	691	1163	138	260	644	3660
SI^{32}	3704	71337	75	366	1393	1392	210	507	988	3660
SI^{64}	3704	144531	150	1156	2346	1696	426	1056	3630	3660

TABLE V
Performance results of four modes of Vocoder in the steady-state.

Mode	Period (T in clk.)	Total utilization (U)	Iteration latency (L)
SI^8	917504	1.24	7339608
SI^{16}	148864	2.36	1191436
SI^{32}	178176	3.19	1425448
SI^{64}	300288	3.4	2402550

from one mode to any other one is possible, thereby resulting in totally 12 possible transitions. At run-time, reconfiguration of the parameter dl is triggered by the environment, e.g., the resource manager in this case. Subsequently, control actor A_c propagates dl to the data-flow actors shown in Fig. 11 through the dashed-lined edges.

We measured the WCETs of all dataflow actors in Fig. 11 in the four modes on an ARM Cortex-A9 [22] processor. All dataflow actors were compiled using the compiler `arm-xilinx-eabi-gcc 4.7.2` with the vectorization option. The WCETs of all actors in all four modes are given in Table IV. It is worth to note that in mode SI^8 , actors `Spec2Env` and `male2female` exhibit exceptionally high WCETs. It is because parameter dl represents the size of the inner-most loop in the computation of actors `Spec2Env` and `male2female`. Small dl (in this case $dl = 8$) leads to the fact that the inner-most loop cannot be vectorized by the compiler. In the other modes from SI^{16} to SI^{64} , larger sizes of the inner-most loop (dl equal to 16, 32, and 64, respectively) lead to full vectorization of the computation of actors `Spec2Env` and `male2female`. Therefore, in these three modes, the WCETs of actors `Spec2Env` and `male2female` are even smaller than the ones in mode SI^8 . The dataflow actors of Vocoder are allocated to 4 PEs as shown in Fig. 12. This allocation guarantees that the shortest periods (maximum throughput) in the steady-states of all modes can be achieved.

Table V shows the performance results for the four modes in their steady-state under SPS. For instance, the second column at the first row in Table V indicates that it is guaranteed for sink actor `WriteWave` to produce 256 samples per 917451 clock cycles in mode SI^8 . This is the “worst-case” performance among all four modes because the `Spec2Env` actor exhibits exceptionally high workload (cf. WCETs in Table IV) in mode SI^8 . Consequently, actor `Spec2Env` becomes the “bottleneck” actor, so that mode SI^8 cannot be scheduled with higher throughput (shorter period). Nevertheless, all mode SI^8 actors as a whole require a total processor utilization (U) of only 1.24 (see the third column in Table V) which is the least among all modes. From Table V, we can see that MADF together with the SPS framework brings another advantage of efficiently utilizing

TABLE VI
Performance results for all mode transitions of Vocoder.

Transition (SI^i to SI^j)	$\Delta_{\min}^{o \rightarrow l}$ (in clk.)	$\Delta_{\max}^{o \rightarrow l}$ (in clk.)	x (in clk.)	$\delta^{o \rightarrow l}$ (in clk.)
$SI^8 \rightarrow SI^{64}$	3636815	4554266	1234264	1234264
$SI^8 \rightarrow SI^{32}$	2903988	3821439	1478540	1478540
$SI^8 \rightarrow SI^{16}$	2728479	3645930	1537043	1537043
$SI^{16} \rightarrow SI^{64}$	2402550	2551480	0	0
$SI^{16} \rightarrow SI^{32}$	1425448	1574378	0	0
$SI^{16} \rightarrow SI^8$	7339608	7488538	0	0
$SI^{32} \rightarrow SI^{64}$	2402550	2580731	0	0
$SI^{32} \rightarrow SI^{16}$	1425448	1603629	234012	234012
$SI^{32} \rightarrow SI^8$	7339608	7517789	0	0
$SI^{64} \rightarrow SI^{32}$	2402550	2702869	977102	977102
$SI^{64} \rightarrow SI^{16}$	2402550	2702869	1211114	1211114
$SI^{64} \rightarrow SI^8$	7339608	7639927	0	0

TABLE VII
The period and iteration latency of modes in MP3 decoder in clk. cycles.

Mode	s-s	s-l	l-s	l-l	m
Period (T)	5830000	5785970	5830000	4640000	5760000
Iteration latency (L)	9434720	9234570	9278600	7466400	9089900

PE resources. For example, in case that Vocoder is switched to a mode with lower processor utilization, idle capacity of PEs can be efficiently utilized by admitting other applications at run-time without introducing interference to the currently running Vocoder.

Now, we focus on the performance results of the MOO protocol, namely transition delays, for all possible transitions between the four modes of Vocoder. Table VI shows both the minimum and maximum transition delays in accordance with Theorem 2 for all transitions. We can see in the second column of Table VI that, in the best case, the transition delays for 6 out of 12 transitions remain the same as the iteration latencies of the new modes. This can be seen as $x = 0$ shown in the fourth column. In these 6 transitions, the proposed MOO protocol does not introduce any extra delay. In the 6 remaining transitions, as expected, the MOO protocol introduces offset $x > 0$ to the transitions from an old mode with a longer iteration latency to a new mode with a shorter iteration latency. For instance, the largest x (in bold shown in Table VI) happens in case of a transition from mode SI^8 with the longest iteration latency (see the fourth column in Table V) to mode SI^{16} with the shortest iteration latency. To quantify x , we compute the percentage of x compared to both minimum and maximum transition delays as

$$\Omega_{\min} = \frac{x}{\Delta_{\min}^{o \rightarrow l}} \times 100\%, \quad \Omega_{\max} = \frac{x}{\Delta_{\max}^{o \rightarrow l}} \times 100\%.$$

Ω_{\min} varies from the worst-case 56% to the best case 16% with an average of 41%, whereas Ω_{\max} varies from the worst-case 44% to the best case 14% with an average of 33%. Therefore, the increase of the transition delays due to the MOO protocol is reasonable for this real-life application.

Next, we consider the effect of the actor allocation shown in Fig. 12 on the earliest starting times of actors in the new mode upon a transition (cf. Lemma 3). In this particular example, we find out that no extra delay is incurred to any actor in all transitions due to the fixed actor allocation. This can be seen from the fourth and fifth columns in Table VI, where $\delta^{o \rightarrow l} = x$.

TABLE VIII
PERFORMANCE RESULTS OF MP3 DECODER FOR FOUR DIFFERENT MODE TRANSITION SEQUENCES USING MADF AND FSM-SADF MODELS.

Mode Sequence	FSM-SADF [5]						MADF							
	Iteration latency			Transition delay			Iteration latency			Transition delay				
	L^{s-s}	L^{s-l}	L^m	L^{l-l}	$\Delta^{s-s \rightarrow s-l}$	$\Delta^{s-l \rightarrow m}$	$\Delta^{m \rightarrow l-l}$	L^{s-s}	L^{s-l}	L^m	L^{l-l}	$\Delta^{s-s \rightarrow s-l}$	$\Delta^{s-l \rightarrow m}$	$\Delta^{m \rightarrow l-l}$
s-s→s-l→m→l-l	9434720	9434670	9310400	9310400	9434670	9310400	9310400	9434720	9234570	9089900	7466400	10032600	9261700	9089900
s-s→l-l→s-l→m	L^{s-s}	L^{l-l}	L^{s-l}	L^m	$\Delta^{s-s \rightarrow l-l}$	$\Delta^{l-l \rightarrow s-l}$	$\Delta^{s-l \rightarrow m}$	L^{s-s}	L^{l-l}	L^{s-l}	L^m	$\Delta^{s-s \rightarrow l-l}$	$\Delta^{l-l \rightarrow s-l}$	$\Delta^{s-l \rightarrow m}$
	9434720	9434700	9434670	9217800	9434700	9434670	9217800	9434720	7466400	9234570	9089900	9434700	9234500	9261700
l-s→s-l→m→l-l	L^{l-s}	L^{s-l}	L^m	L^{l-l}	$\Delta^{l-s \rightarrow s-l}$	$\Delta^{s-l \rightarrow m}$	$\Delta^{m \rightarrow l-l}$	L^{l-s}	L^{s-l}	L^m	L^{l-l}	$\Delta^{l-s \rightarrow s-l}$	$\Delta^{s-l \rightarrow m}$	$\Delta^{m \rightarrow l-l}$
	9278600	9278570	9197200	9197200	9278570	9197200	9197200	9278600	9234570	9089900	7466400	9876500	9261700	9089900
s-s→l-s→s-l→l-l	L^{s-s}	L^{l-s}	L^{s-l}	L^{l-l}	$\Delta^{s-s \rightarrow l-s}$	$\Delta^{l-s \rightarrow s-l}$	$\Delta^{s-l \rightarrow l-l}$	L^{s-s}	L^{l-s}	L^{s-l}	L^{l-l}	$\Delta^{s-s \rightarrow l-s}$	$\Delta^{l-s \rightarrow s-l}$	$\Delta^{s-l \rightarrow l-l}$
	9434720	9434700	9434670	8661500	9434700	9434670	8661500	9434720	9278600	9234570	7466400	10032600	9876500	9234600

B. Case Study 2

To further evaluate the MOO protocol, presented in Section IV-C2, in this section, we performed an experiment with the MP3 decoder application, which is a real-life adaptive streaming application, taken from [5]. This MP3 decoder is a frame-based algorithm that retrieves audio frames from the incoming compressed bitstream. In the MP3 decoder, each audio frame can be decoded using a different method. In total, MP3 decoder has five individual decoding methods for audio frames that are denoted as {s-s, l-l, l-s, s-l, m}.

Each of these methods can be represented accurately by an SDF graph. Therefore, the application behavior can be accurately captured using FSM-SADF [5] rather than conservatively capture these methods in a static dataflow model. Consequently, a much tighter performance can be guaranteed by FSM-SADF graph than SDF. Note that since each mode in our MADF model is represented as a CSDF graph, our MADF is more expressive than FSM-SADF and therefore, the MP3 decoder can be also properly modeled with MADF. The period and iteration latency of each mode are given in Table VII.

Let us now compare the throughput of MP3 decoder modeled as MADF and FSM-SADF graphs. To compute the throughput of MP3 decoder modeled by the FSM-SADF, we use the publicly available SDF³ tool set [23]. Since the type of frames may change non-deterministically in arbitrary orders, SDF³ detects the worst-case mode transition using the state-space exploration approach developed in [5] for FSM-SADF to lower bound the throughput. To compute the worst-case throughput of the application, we use the `sdf3analysis-fsmsadf` tool from SDF³. Similarly, we use the same approach to compute the throughput of our MADF model that uses the MOO protocol. For both models, the same throughput of $1.75 \cdot 10^{-7}$ frame per clock cycle is achieved. Therefore, both models perform equally well in terms of the worst-case throughput they can guarantee and the delay introduced by our MOO protocol during mode transitions has no impact on the worst-case throughput.

Now, we focus on the performance results of our MADF and FSM-SADF models in terms of the iteration latency of the modes and the transition delay. The results of this comparison for four different mode transition sequences is given in Table VIII. In this table, for each mode transition sequence, the iteration latency of each mode and the transition delay of each mode transition are given for our MADF model that uses the MOO protocol and the FSM-SADF model that uses the self-timed protocol. From this table, we can clearly see that our MADF retains the iteration latency of each mode irrespective of

the mode transition sequences. Using the FSM-SADF model, however, the iteration latency of modes in the steady-state is accordingly changed with respect to the order of mode transitions. For instance, mode l-l has different iteration latency, L^{l-l} , of 9310400, 9434700, 9197200, and 8661500 for the different mode transition sequences, when using FSM-SADF. In contrast, the same mode l-l has a constant iteration latency of 7466400 under our MADF model (bolded in Table VIII). Therefore, the iteration latency of modes in the steady-state can not be guaranteed under the FSM-SADF model as it is highly dependent on the order of mode transitions which is not known beforehand at design-time.

From Table VIII, we can also see that by changing the iteration latency of the modes, the transition delays are also changed. Although the transition delays are sometimes shorter in the FSM-SADF model, the FSM-SADF model is potentially unpredictable. Our MADF model, however, is completely predictable because the (minimum) transition delays for all mode transitions can be computed beforehand at design-time according to Theorem 2. For instance, the transition from mode s-l to mode m has different transition delay, $\Delta^{s-l \rightarrow m}$, of 9310400, 9217800, and 9197200 for different mode transition sequences under the FSM-SADF model whereas this mode transition has a constant transition delay of 9261700 under our MADF model (bolded in Table VIII).

VII. CONCLUSION

In this paper, we have proposed the novel Mode-Aware Data Flow (MADF) model which can capture effectively the adaptive nature of modern streaming applications. Moreover, as an important part of the operational semantics of MADF, we have proposed a novel protocol for mode transitions. The main advantage of this transition protocol is that, in contrast to the self-timed transition protocol, it avoids timing interference between modes upon mode transitions. As a result, any mode transition can be analyzed independently from others that occurred in the past. Furthermore, based on the transition protocol, we have proposed a hard real-time analysis and scheduling framework to reason and guarantee timing constraints by avoiding processor overloading during mode transitions. Finally, we evaluate the effectiveness of our MADF model compared with the well-know FSM-SADF model by conducting two case studies using two real-life adaptive streaming applications.

REFERENCES

- [1] A. Gerstlauer et al. Electronic system-level synthesis methodologies. *IEEE Trans. Comput.-Aided Design Integr. Circuits Syst.*, 2009.
- [2] E. A. Lee and D. G. Messerschmitt. Static scheduling of synchronous data flow programs for digital signal processing. *IEEE Trans. on computers*, 1987.
- [3] G. Bilsen et al. Cycle-static dataflow. *IEEE Trans. Signal Process.*, 1996.
- [4] B. D. Theelen et al. A scenario-aware data flow model for combined long-run average and worst-case performance analysis. In *MEMOCODE*, 2006.
- [5] M. Geilen and S. Stuijk. Worst-case performance analysis of synchronous dataflow scenarios. In *CODES+ISSS*, 2010.
- [6] M. H. Wiggers et al. Buffer capacity computation for throughput-constrained modal task graphs. *ACM Trans. Embed. Comput. Syst.*, 2010.
- [7] O. Moreira. Temporal analysis and scheduling of hard real-time radios running on a multi-processor. *ser. PHD Thesis, Technische Universiteit Eindhoven*, 2012.
- [8] B. Bhattacharya and S. S. Bhattacharyya. Parameterized dataflow modeling for dsp systems. *IEEE Trans. Signal Process.*, 2001.
- [9] M. Geilen. Synchronous dataflow scenarios. *ACM Trans. Embed. Comput. Syst.*, 2010.
- [10] R. Henia and R. Ernst. Scenario aware analysis for complex event models and distributed systems. In *RTSS*, 2007.
- [11] M. Negrean et al. Bounding mode change transition latencies for multi-mode real-time distributed applications. In *ETFA*, 2011.
- [12] J. Real and A.s Crespo. Mode change protocols for real-time systems: A survey and a new proposal. *Real-time Systems*, 2004.
- [13] N. Stoimenov et al. Reliable mode changes in real-time systems with fixed priority or edf scheduling. In *DATE*, 2009.
- [14] M. Bamakhrama and T. Stefanov. On the hard-real-time scheduling of embedded streaming applications. *DAES*, 2013.
- [15] B. Lickly et al. Predictable programming on a precision timed architecture. In *CASES*, 2008.
- [16] C. L. Liu and J. W. Layland. Scheduling algorithms for multiprogramming in a hard-real-time environment. *Journal of the ACM (JACM)*, 1973.
- [17] S. Stuijk et al. Throughput-buffering trade-off exploration for cyclo-static and synchronous dataflow graphs. *IEEE Trans. on Computers*, 2008.
- [18] B. Bodin et al. Periodic schedules for cyclo-static dataflow. In *ESTIMedia*, 2013.
- [19] S. Neuendorffer and E. Lee. Hierarchical reconfiguration of dataflow models. In *MEMOCODE*, 2004.
- [20] S. Niknam and T. Stefanov. Energy-efficient scheduling of throughput-constrained streaming applications by periodic mode switching. In *SAMOS*, 2017.
- [21] M. I. Gordon, W. Thies, and S. Amarasinghe. Exploiting coarse-grained task, data, and pipeline parallelism in stream programs. *ACM SIGOPS Operating Systems Review*, 2006.
- [22] ARM Cortex. A9 processor. <http://www.arm.com/products/processors/cortex-a/cortex-a9.php>, 2013.
- [23] S. Stuijk, M. Geilen, and T. Basten. Sdf^{*} 3: Sdf for free. In *ACSD*, 2006.



Jiali Teddy Zhai was born on 16th of October, 1982. In September 2009, he received Diplom Informatik (Master Degree in Computer Science) from Friedrich-Alexander Universitat Erlangen-Nurnberg, Germany. During his study, Teddy worked at Institute for Hardware-Software-Co-Design headed by Prof. Jürgen Teich with the focus on designing high-level synthesis tools targeting high-performance computing systems based on FPGA platforms. In October 2009, Teddy joined the Leiden Embedded Research Center (LERC) which is part of the Leiden Institute of

Advanced Computer Science (LIACS) at Leiden University. He was appointed as a research and teaching assistant (Ph.D. student). He was involved in the NETHERLANDS STREAMING (NEST) project in collaboration with NXP semiconductor, Philips Healthcare, etc. In April 2014 Teddy joined Irdeto B.V. Netherlands as Senior Security Engineer. From June 2016 on, Teddy has been appointed by Green Hills Software Netherlands as Security Solution Architect, Europe.



systems design.

Sobhan Niknam received his B.Sc. and M.Sc. degrees in computer engineering from Shahed University and Iran University of Science and Technology both in Tehran, Iran, in 2012 and 2014, respectively. Since March 2015, he has been with the Leiden Embedded Research Center (LERC) which is part of the Leiden Institute of Advanced Computer Science (LIACS) at Leiden University in The Netherlands, where he is working toward the Ph.D. degree in computer science. His research interests include real-time embedded systems and system-level multi-core



Todor Stefanov (S'01–M'05) received the Dipl.Ing. and M.S. degrees in computer engineering from The Technical University of Sofia, Bulgaria, in 1998 and the Ph.D. degree in computer science from Leiden University, The Netherlands, in 2004. Currently, he is an associate professor in the Leiden Institute of Advanced Computer Science at Leiden University and the head of the Leiden Embedded Research Center (LERC) which is a medium-size research group with a strong track record in the area of system-level modeling and synthesis, programming, and implementation of heterogeneous embedded systems. Dr. Stefanov is a recipient of the prestigious 2009 IEEE TCAD DONALD O.PEDERSON BEST PAPER AWARD for his journal article "Systematic and Automated Multi-processor System Design, Programming, and Implementation" published in the IEEE Transactions on Computer-Aided Design of Integrated Circuits and Systems (TCAD). He is editorial board member of the Springer Journal on Embedded Systems. He has also been editorial board member of the International Journal of Reconfigurable Computing and guest associate editor of ACM Transactions on Embedded Computing Systems (2013). He has been General Chair of ESTIMedia 2015 and Local Organization Co-Chair of ESWeek 2015. Moreover, he serves (has served) on the organizational committees of several leading conferences, symposia, and workshops, such as DATE, ACM/IEEE CODES+ISSS, RTSS, IEEE ICCD, IEEE/IFIP VLSI-SoC, ESTIMedia, SAMOS (as TPC member), and IEEE ESTIMedia, ACM SCOPES (as Program Chair). Dr. Stefanov (co-)authored more than 80 scientific papers. His research interests include several aspects of embedded systems design, with particular emphasis on system-level design automation, multiprocessor systems-on-chip design, and hardware/software co-design.